Heterogeneously catalysed partial oxidation of acrolein to acrylic acid—structure, function and dynamics of the V–Mo–W mixed oxides†

Philip Kampe,[a] Lars Giebeler,[b] Dominik Samuelis,[c] Jan Kunert,[a] Alfons Drochner,[a] Frank Haaß,[bc] Andreas H. Adams,[b] Joerg Ott,[a] Silvia Endres,[a] Guido Schimanke,[c] Thorsten Buhrmester,[b] Manfred Martin,*[c] Hartmut Fuess*[b] and Herbert Vogel*[a]

Received 4th January 2007, Accepted 2nd April 2007
First published as an Advance Article on the web 26th April 2007
DOI: 10.1039/b700098g

The major objective of this research project was to reach a microscopic understanding of the structure, function and dynamics of V–Mo–(W) mixed oxides for the partial oxidation of acrolein to acrylic acid. Different model catalysts (from binary and ternary vanadium molybdenum oxides up to quaternary oxides with additional tungsten) were prepared *via* a solid state preparation route and hydrochemical preparation of precursors by spray-drying or crystallisation with subsequent calcination. The phase composition was investigated *ex situ* by XRD and HR-TEM. Solid state prepared samples are characterised by crystalline phases associated to suitable phase diagrams. Samples prepared from crystallised and spray-dried precursors show crystalline phases which are not part of the phase diagram. Amorphous or nanocrystalline structures are only found in tungsten doped samples. The kinetics of the partial oxidation as well as the catalysts' structure have been studied *in situ* by XAS, XRD, temperature programmed reaction and reduction as well as by a transient isotopic tracing technique (SSITKA). The reduction and re-oxidation kinetics of the bulk phase have been evaluated by XAS. A direct influence not only of the catalysts' composition but also of the preparation route is shown. Altogether correlations are drawn between structure, oxygen dynamics and the catalytic performance in terms of activity, selectivity and long-term stability. A model for the solid state behaviour under reaction conditions has been developed. Furthermore, isotope exchange experiments provided a closer image of the mechanism of the selective acrolein oxidation. Based on the *in situ* characterisation in combination with micro kinetic modelling a detailed reaction model which describes the oxygen exchange and the processes at the catalyst more precisely is discussed.

Introduction

This work was part of the priority programme of the German Research Foundation (DFG) "Bridging the gap between ideal and real systems in heterogeneous catalysis". Therein, the thermodynamics, kinetics and dynamics of several technically relevant catalytic systems were investigated. The philosophy of this approach was to answer the question: to what extent is it possible to extrapolate results from single crystal under UHV to the complex catalyst working under industrial conditions? We investigated the technically important selective oxidation of acrolein to acrylic acid. The aim was not to improve the industrial catalyst but to gain a better scientific understanding of the structure, function and dynamics of the catalyst based on V–Mo mixed oxides. For this, it was essential to find a model catalyst as simple as possible that still provides the key features (activity, selectivity, stability). To bridge the gap between ideal and real systems, different model catalysts (from the pure crystalline oxides to the amorphous V–Mo–W mixed oxides) were studied extensively using several probe molecules (from H_2 *via* CO to acrolein) in the whole pressure range (from UHV *via* inert gas to reaction gas under atmospheric pressure).

History of acrylic acid synthesis

Acrylic acid (AA) is, from a chemical point of view, the simplest unsaturated monocarboxylic acid. The most striking chemical property is its extraordinary propensity for polymerisation, therefore handling during synthesis, storage, transport and work up requires great care and sophisticated knowledge.[1]

AA is the intermediate for the production of:

- Acrylic esters (53%‡) (especially methyl-, ethyl-, *n*-butyl- and 2-ethylhexyl-)
- Superabsorber polymers (31%)
- Detergents (6%)

[a] *Darmstadt University of Technology, Faculty of Chemistry, Technical Chemistry, Petersenstr. 20, D-64287 Darmstadt, Germany. E-mail: vogel@ct.chemie.tu-darmstadt.de; Fax: +49 6151 163465; Tel: +49 6151 162165*
[b] *Darmstadt University of Technology, Institute for Materials Science Structure Research, Petersenstr. 23, D-64287 Darmstadt, Germany. E-mail: hfuess@tu-darmstadt.de; Fax: +49 6151 166023; Tel: +49 6151 164373*
[c] *RWTH Aachen University, Institute of Physical Chemistry, Landoltweg 2, D-52074 Aachen, Germany. E-mail: martin@pc.rwth-aachen.de; Fax: +49 241 80992128; Tel: +49 241 8094712*

† Electronic supplementary information (ESI) available: *In situ* XANES spectra. See DOI: 10.1039/b700098g

‡ These data refer to the US consumption in the year 2000.

- Water treatment agents (3%)
- Other (7%).

In recent years, the increase in the consumption rate of AA has been the most pronounced of all unsaturated organic acids. Above all, this is due to the strong increase in the demand for superabsorber polymers (*ca.* 7% growth per year over the last three years), that are produced by Dow Chemicals and BASF. The current world capacity amounts to approx. 3.4 million tons per year (1994 approx. 2.0 million tons per year, 1985 approx. 1.0 million tons per year). The world's biggest producer is BASF. Currently, a worldscale plant has a capacity of almost 200 000 tons per year.

AA has been produced commercially since 1920. Starting from the first technical AA production by Röhm and Haas in Darmstadt, Germany, five technical processes have been carried out:

- Ethylencyanhydrine process
- Acrylonitrile process
- Reppe process
- Ketene- or propiolactone process
- Propene process.

The change of the raw material basis of the chemical industry from coal to oil in the 1950s was the driving force for the adjustment of the process routes for many intermediates such as AA. Thus, until the 1970s, AA was mainly produced by the Reppe process *via* homogeneous catalytic conversion of acetylene (coal → carbide → acetylene) with CO/H_2O. The increasingly less expensive propylene from the steam cracker, was the main driving force for the development of catalysts and processes for the partial oxidation of propylene with molecular oxygen to AA. Thus, the first attempts took place in the beginning of the 1960s to convert propylene in one step with Sohio's (now part of BP) acrylonitrile catalyst (Mo–Bi mixed oxide). The yields achieved were a modest 35%. In the following years, an exemplary catalyst development began with the steps:[2–4]

- Splitting the synthesis into two steps (propene → acrolein (ACR) → AA)
- Optimisation of the catalyst system for each step:
- From Mo–W–Fe to Mo–Bi–Fe–Ni-mixed oxide (1st step)
- From Mo–W–Fe to Mo–W–V–Fe-mixed oxide (2nd step)
- From bulk to shell catalysts
- Changing the shape from spheres to tablets, from tablets to rings.

With today's technological AA catalysts, yields of about 90% are achieved within both steps and operating times of some years. In contrast to this excellent catalyst performance, the understanding of the reaction mechanism is rather modest. The catalyst development was based on trial and error and did not differ substantially from the procedure that was common in the time of Alwin Mittasch (1869–1953) during the development of ammonia and methanol catalysts. Only in recent times have attempts been made to understand the mode of action of the catalytic system with a rational approach in order to transfer this knowledge base to other systems (*e.g.* the partial oxidation of methacrolein). While this has already succeeded to a large extent with the first step (propene → ACR), the understanding of the catalytic mechanism of the second step (ACR → AA) is incomplete. Therefore the main intention of this project was to investigate the catalytic material by a combination of methods and thus contribute to a detailed understanding of the mechanism of this reaction.

Transition metal oxides and their function in selective oxidations

For selective oxidations, transition metal oxides are used as catalysts. The metal ions can easily change their oxidation states and can, therefore, act as redox centres during oxidation and reduction of the substrate and the catalyst. Unlike metallic catalysts, the oxygen, which is bound in the catalyst, is an active reaction partner and can be released to the substrate. The re-oxidation of the catalyst occurs separately with an external oxygen source (*e.g.* molecular oxygen). Thus, all in all, the catalyst remains unchanged. This generally accepted model for the processing of heterogeneously catalysed partial oxidations is known as the "Mars–van Krevelen mechanism".[5]

Investigations on the different industrially applied catalysts—that have been optimised by the various companies *via* numerous promoters (W, Cu, Mn, Fe, Sb, Cr, Sr are among them)[4]—promise little for the understanding of the underlying mechanisms due to their complexity. For this reason the research activities were focussed on model systems based on fewer components, whose number was gradually increased according to progressive knowledge. However, a minimum number of necessary components from which an active, selective and stable catalyst can be composed is given by the single reaction steps that a selective and active catalyst should accelerate:[6] the chemisorption of the substrates and the reaction with oxygen *via* a coordinatively unsaturated multivalent metal species with covalent character in its highest oxidation state (*e.g.* Mo^{VI}), as well as the activation of the C–H bond (*e.g.* vanadium, as for alkane activation).[7–9]

V–Mo–W mixed oxides as model catalysts for acrolein oxidation

V–Mo mixed oxides, which are generally available as complex multiphase systems, form the basis for the catalyst system for the ACR oxidation. A number of thermodynamically stable modifications exist which are synthesised *via* melting at high temperatures. The phase diagram for these stable mixed oxides which only displays two mixed oxide phases (α and β phases)[10] as well as the pure oxides MoO_3 and V_2O_5 is known in literature.

Important for catalysis are the low temperature modifications, which can be synthesised *via* precursor routes, *e.g.* from the ammonia salts of the corresponding heteropoly acids at temperatures up to 400 °C.[11,12] The employment of a fast drying method during the precursor synthesis has a supporting effect on the formation of metastable phases. The industrial catalyst production is therefore based on spray-drying which yields a large proportion of X-ray amorphous material.[13]

Mixed oxides with a V–Mo ratio of about 1 : 3 have proven to be particularly active and selective.[14] Higher proportions of V lead to lower selectivity with higher activity. In contrast, pure molybdenum oxide is almost inactive.

The structure of the V–Mo–(W) mixed oxides and the search for the active phases are the subject of various

investigations. Andrushkevich postulated that Mo_3VO_{11} is the active and selective phase.[14] Conversely, Schlögl *et al.* suggest Mo_4VO_{14} as the active and selective phase, which they support with numerous investigations.[15,16] Although the phases put forward by Andrushkevich and Schlögl exhibit a very similar oxygen to metal ratio (2.75 and 2.8), their structures show clear differences.

In a ternary V–Mo mixed oxide, the metastable structures are not stable at higher temperatures. As an example, calcination leads to phase transitions, amorphous parts are converted into crystalline parts. It appears that the addition of W even in small amounts has a stabilising influence. This can already be recognised during the preparation and manifests itself as an increase in the X-ray amorphous phases.[11] Due to its high oxygen bonding strength, in comparison with Mo and V, there is a high probability that W is not directly involved in the oxygen transfer process, but essentially works as a structural promoter. In other industrially used catalysts, niobium is used instead of W, which has a similar effect.[17]

Function of solid state oxygen

Different theories exist as to which synergistic effects lead to the preference of selective oxidation as opposed to the competing total oxidation. High selectivities can be achieved *via* an oxygen limitation of the active centre (→ site isolation concept).[18,19] Therefore, insufficient oxygen is available for the total oxidation. This limitation can be realised by a careful adjustment of the degree of reduction, or by the isolation of the active phase using inactive phases. The available oxygen can also be limited by its transport to the corresponding active centre. This is the concept of phase cooperation,[20] where oxygen species are transferred from the oxygen donor phase to the oxygen acceptor phase, possibly by surface migration or bulk diffusion. Slight anomalies in the structures lead to small surface energies and allow the transport of O^{2-} ions through the phase boundary.[18] Often the so-called core-shell or cherry-like model are found in the literature:[21] on the surface there is a phase that provides a large number of active centres. The bulk phase is characterised by high electronic conductivity and ion mobility. Very few publications contain detailed information on the surface intermediates arising during the partial oxidation. A detailed suggestion for the reaction mechanism of ACR oxidation was published by Andrushkevich.[14] The author proposed a detailed mechanism of the selective oxidation to AA based on IR spectroscopy and TPD measurements. From these data she derived the formation of active surface species and their conversion during the reaction. In the first stage the carbonyl interacts with a molybdenum cation. The most important intermediates arising are a covalently bound complex of solid oxygen and the carbonyl group (asymmetric acrylate complex) as well as an ionic acrylate complex bound to V^{IV}. Intermediates that lead to total oxidation products are not shown by Andrushkevich's mechanism.

Model system—reduction of chemical complexity

Multifunctional catalysts are a prerequisite for heterogeneously catalysed partial oxidations. Both the organic molecule and the oxygen have to be activated simultaneously but at different active sites. Furthermore the regeneration of the catalyst is mandatory if the oxygen originates from the solid. In the present study the function and dynamics of V–Mo mixed oxides during selective oxidation of aldehydes are investigated. However, the focus of this study is a detailed understanding of the function of the industrially used catalyst with a rational approach in mind, rather than its optimisation. The reaction mechanism comprises different adsorption and desorption steps, dissociation of oxygen and surface diffusion as well as the surface reaction to form AA (Fig. 1). On a macroscopic scale it can be described by the Mars–van Krevelen mechanism,[5] but on a microscopic scale, the single steps of the mechanism are not yet known in detail and not even the active sites have been identified unambigously.

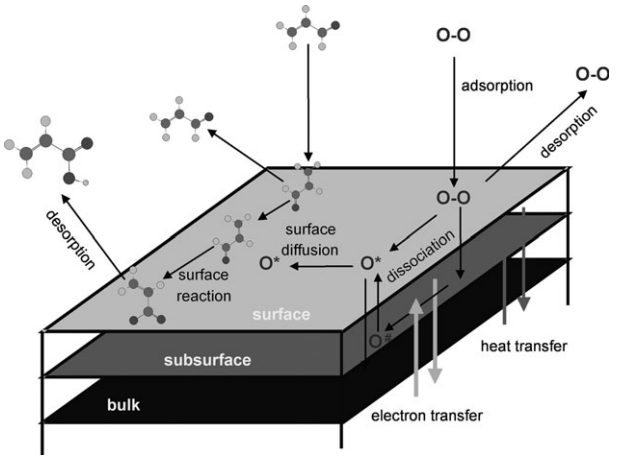

Fig. 1 Reaction scheme with different adsorption and desorption steps, dissociation of oxygen and surface diffusion as well as the surface reaction to AA.

The composition of the catalyst used in industry is empirically acquired and a lot of promoters are added.[4] For scientific research the complexity has to be reduced to a reasonable level. The question is, to what extent can the solid's complexity be reduced without losing the crucial properties—activity, selectivity and long-term stability. Is there any relation between the properties of a single phase pure oxide like MoO_3 or V_2O_5 and the real multiphase catalyst? Furthermore, is it possible to substitute the aldehyde by simpler probe molecules such as carbon monoxide or hydrogen?

To consider these questions several research techniques were applied in the pressure range from UHV over inert gas to real catalytic conditions, from electron microscopy and XPS over X-ray diffraction, X-ray absorption spectroscopy (XAS), and infrared spectroscopy up to temperature and concentration programmed methods as well as isotope exchange experiments.

Preparation and characterisation of the catalysts (materials gap)

Within the materials gap, the influence of different preparation strategies and of a varied metal to metal ratio on the structure and morphology of the mixed oxides was investigated. Several model substances in the whole range from the

thermodynamically stable pure oxides to the ternary oxides up to the quaternary model system for the industrial catalyst were prepared and analysed.

The first sample series consists of ternary V–Mo mixed oxides with the composition $V_{1-x}Mo_xO_z$ ($0 \leq x \leq 1$, z = charge balance). Therefore a reproducible and suitable preparation strategy was developed to separate different parameters and evaluate their influence on the oxides and their catalytic performance.[11] A second series of quaternary mixed oxides with W as an additional dopant was prepared with the general stoichiometry $V_2Mo_8W_yO_z$ ($0 \leq y \leq 5$). All samples were analysed by X-ray fluorescence analysis (RFA) and the employed contents of the metals were confirmed. Temperature programmed (TP) reactions were conducted to calculate the catalysts' performance under industry-like conditions.

Preparation techniques for mixed oxide catalysts

The preparation of the catalysts and model substances was performed by two different methods:

Solid state preparation. The first oxide series were prepared by melting and calcining the binary oxides MoO_3, V_2O_5 and WO_3 in the desired stoichiometry to obtain materials with thermodynamically stable phases. Therefore, the oxides were homogenised in an agate mortar and melted in a sealed vacuum quartz tube. Then the powder was pressed into pellets and was annealed in a muffle furnace for seven days at 600 °C. After the calcination procedure the pellets were quenched in liquid nitrogen to stabilise the crystalline phases formed. The details of the solid state preparation can be found in Adams *et al.*[22,23]

Hydrochemical preparation routes. The second method of preparation is based on aqueous solutions of the ammonium salts acidified with nitric acid. To prepare the oxides, the precursor solutions were dried *via* crystallisation and spray-drying. The obtained powder was treated in a special furnace with an annealing programme up to 400 °C as the maximum temperature. The preparation of the oxides through aqueous solutions can be found in Kunert *et al.*[12]

Characterisation of the prepared model systems (*ex situ*)

The phase compositions were examined by X-ray diffraction (XRD) with subsequent Rietveld refinement. The XRD patterns of the solid state prepared samples show crystalline structures (Fig. 2).

The phase composition of the W-free sample series depends on the Mo content. Orthorhombic V_2O_5 structure type, space group (SG) *Pmmn*,[24] is stable until a Mo concentration of $x \leq 0.08$ assigned to the stoichiometry $(V_{1-x}Mo_x)_2O_5$. In the range of $0.08 < x < 0.40$ a biphasic system of orthorhombic V_2O_5 and monoclinic V_2MoO_8 structure types, SG *C*2,[25] exists. At a Mo concentration of $x \geq 0.40$ monoclinic V_2MoO_8 and orthorhombic MoO_3, SG *Pbnm*,[26] are found, except $x = 1$.

The $V_2Mo_8W_yO_z$ ($0 \leq y \leq 5$) system shows a phase composition similar to the ternary oxides at a W content $y = 0$. In the region with low W contents $0.5 \leq y \leq 2$ the orthorhombic $Mo_{0.6}W_{0.4}O_3$ structure type as an additional W containing phase is found. A four-phase system is observed at

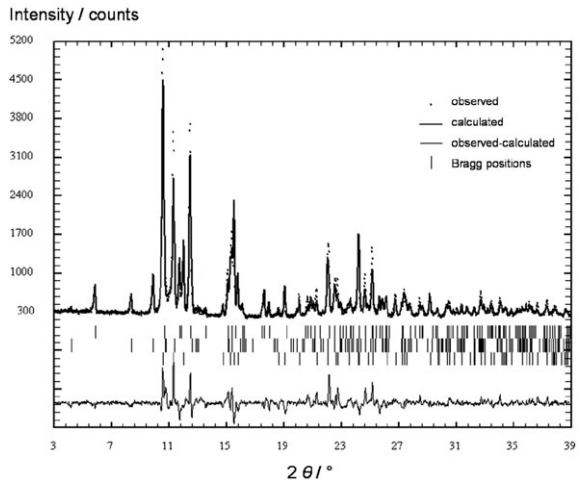

Fig. 2 XRD pattern and Rietveld refinement of the sample $V_2Mo_8W_{1,5}O_z$. The Bragg positions of the phases from top to bottom are orthorhombic MoO_3, monoclinic V_2MoO_8 and orthorhombic $Mo_{0.6}W_{0.4}O_3$.

W contents of $y > 2$. The fourth phase has a monoclinic $Mo_{0.29}W_{0.71}O_3$ structure type, SG $P2_1/n$.[27] The main phases at lower W content are orthorhombic MoO_3 and monoclinic V_2MoO_8 types. At higher W content V_2MoO_8 and monoclinic $Mo_{0.29}W_{0.71}O_3$ types also dominate.

The comparison of the phases in the two sample series with the phase diagrams of V_2O_5–MoO_3[10] and MoO_3–WO_3[27] reveals only the presence of thermodynamically stable phases.

The catalysts prepared *via* hydrochemical methods displays different phase compositions compared to the ones prepared by the solid state method. The main components for the W-free crystallised and spray-dried catalysts are the crystalline phases of the hexagonal $(V,Mo)O_3$, SG $P6_3$,[28] and triclinic $(V,Mo)_2O_5$ structure types, SG $P1$.[29] Orthorhombic MoO_3 is found in samples with high Mo contents $0.9 \leq x \leq 1$ for the crystallised and at $x = 1$ for the spray-dried samples.[23] The spray-dried sample with Mo content $x = 1$ contains monoclinic V_6O_{13}, SG $C2/m$,[30] and orthorhombic V_2O_5 types.

The crystallised quaternary V–Mo–W mixed oxide catalysts exhibit crystalline structures in the XRD pattern. Changes occur at a W content of $y = 5$. This is the point of a significant decrease in particle size as indicated by the broadening of the reflexes, the structures in the XRD pattern change from crystalline to amorphous/nanocrystalline. It should be noted that this is not an abrupt transformation. It sets in at $y = 4$ as evidenced by the higher background of the diffractogram compared to samples with W contents of $y < 4$.[31] The crystalline parts of the sample with $y = 4$ are fitted well by the Rietveld refinement.

The spray-dried catalysts with a W content of $0 \leq y \leq 1$ have similar patterns as those mentioned for the crystallised catalysts. At $y > 1$ an abrupt change in crystallinity is observed. All patterns show that spray-dried samples with high W contents have transformed from crystalline to amorphous/nanocrystalline.[31]

The phase composition of the crystalline samples of both preparation methods is comparable. Hexagonal $(V,Mo)O_3$

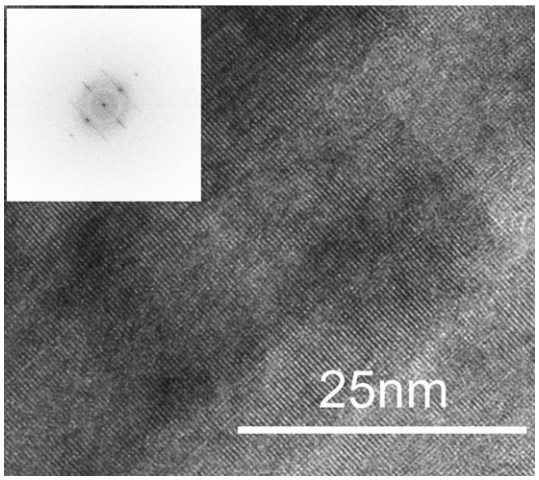

Fig. 3 High-resolution image of tetragonal Mo_5O_{14} structure and the FFT of the HR-TEM image.

and triclinic $(V,Mo)_2O_5$ structure types are the main phases.[31] The observation of the hexagonal WO_3 type, SG *P6/mmm*,[32] as an additional phase is closely related to the increasing W content. In the spray-dried samples a higher purity of the phase composition can be observed with hexagonal $(V,Mo)O_3$ as the main phase.

For the amorphous/nanocrystalline catalysts orthorhombic MoO_3 and tetragonal Mo_5O_{14} structure types, SG *P4/mbm*,[33] are found exclusively by Rietveld refinement. These phases were confirmed by transmission electron microscopy (TEM) especially for the Mo_5O_{14} structure. Amorphous/nanocrystalline Mo_5O_{14} is characterised by rectangular rods in the image (Fig. 3). These rods form a pseudo-lamellar structure. In the fast Fourier transform (FFT) inset in Fig. 3, the analysis of the streaks results in distances of 3.9 ± 0.1 Å. The value corresponds to the literature data[33] of 3.937 Å for the Mo_5O_{14} structure in direction of the *c*-axis. This result is supported in the literature by a comparable V–Mo–W mixed oxide catalyst doped with Cs and P.[34]

The oxidation states of the metals in the catalysts before reaction were determined to be +6 for Mo and W and +4 and +5 for V by XPS. Dependent on the W content *y*, the proportion of the V oxidation states varies for both preparation methods. Other oxidation states like V^{3+} or Mo^{5+}/W^{5+} are absent. In summary, the XPS data (Tables 1 and 2) support the results of XRD and TEM.

From H_2 and CO to acrolein (probes gap)

In many studies H_2 or CO are employed as simple and easy to handle reducing agents. In particular, with H_2 as the reducing agent the formation of a coke layer is avoided. However, the question remains as to whether the results for the redox behaviour obtained with these probe molecules can be transferred to the behaviour of the mixed oxides under an ACR atmosphere. The thermograms of TP reduction with hydrogen and ACR (Fig. 4) point out that information about the redox activity of V–Mo mixed oxides under a hydrogen atmosphere cannot be transferred to the behaviour under ACR, as is clearly indicated by the differential thermogravimetric signal.

Table 1 Binding energies of the determined ions, dependent on tungsten content *y* and reaction conditions for the crystallised catalysts

$V_2Mo_8W_yO_z$	Binding energies/eV			
y	V^{5+}/V^{4+} $2p_{3/2}$	Mo^{6+} $3d_{5/2}$	W^{6+} $4f_{7/2}$	O^{2-} 1s
0	517.1/516	232.6	—	530.4
1.5	517.2/516.1	232.7	35.2	530.5
3	517.1/516	232.7	35.1	530.5
5	517.3/516.2	232.6	35.2	530.6
	After reaction/re-oxidation			
3 after reaction	517.2/516.2	232.4	35.7	530.4
3 after re-oxidation	517.1/516.1	232.5	35.7	530.4

CO is not a suitable probe molecule either. Under steady state conditions in the temperature range from 315–375 °C CO is not oxidised on the V–Mo–W mixed oxides (Fig. 5). Furthermore, as could be shown by isotope exchange experiments with $^{18}O_2$ in the feed gas, no oxygen exchange between CO and the catalyst takes place.[35]

XAS analysis of catalyst samples with CO as a probe molecule was carried out at the Mo K edge.[36] The catalyst's Mo^{6+} ions are reduced to Mo^{4+} by means of CO. However, the reduction was only achieved within a period of several hours at temperatures around 500 °C. Successive re-oxidation with O_2 yields the initial structure, with a Mo oxidation state very close to Mo^{6+}. The characteristic time for reduction is approx. 10 times longer than that for re-oxidation.

In further TP reactions and isotope exchange experiments with the saturated propionaldehyde the activity of V–Mo–W mixed oxides for the oxidation of propionaldehyde was found to be higher compared to the oxidation of acrolein, accompanied with a lower selectivity to propanoic acid.[35] However, these results and results from isotope exchange experiments (discussed later) indicate that the allylic double bond in acrolein does not play a crucial role in the partial oxidation.

The working catalyst—dependency on reaction conditions (pressure gap)

Reductive conditions

***In situ* characterisation of the model catalyst.** The performance of the catalysts was characterised by TP experiments in

Table 2 Amount of V^{4+} and V^{5+} for the crystallised catalysts dependent on the tungsten content *y* and the reaction conditions

$V_2Mo_8W_yO_z$ *y*	Crystallised V^{5+}/V^{4+} (%)
0	67/33
1.5	58/42
3	61/39
5	34/66
	After reaction/re-oxidation
3 after reaction	35/65
3 after re-oxidation	45/55

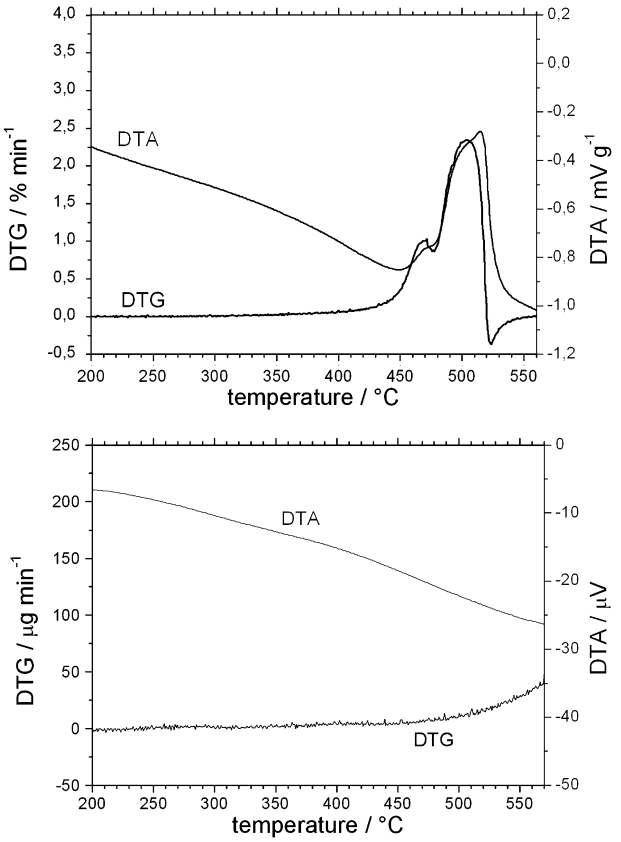

Fig. 4 Differential thermoanalysis (DTA) and differential thermogravimetry (DTG) of TP reduction with ACR (top) and H_2 (bottom).

a microreactor with ACR as reducing agent. The design of the equipment was published by Böhling *et al.*[37] The gas mixing unit contains a gas saturator system for dosing the liquid components. The quartz glass reactor is fixed in an electrically heated oven. The reaction products were analysed by a quadrupole mass spectrometer (InProcess, GAM 400). A continuous analysis of ACR, oxygen, AA, carbon dioxide, carbon monoxide and water was achieved through online monitoring.

For TP reductions 50 mg of a probe were pre-treated at 400 °C for 60 min with 10 vol% oxygen (Messer Griesheim) in inert gas with a flow rate of 1.2 l h^{-1} and subsequently cooled down to room temperature in inert gas. Argon (Messer Griesheim) was used as the inert gas.

The TP reductions were carried out with 5 vol% ACR (BASF), balance argon. The temperature was raised with a constant heating rate of 10 °C min^{-1} to a maximum of 480 °C and cooled down to 400 °C followed by a re-oxidation of the catalyst under the conditions of the pre-treatment. The reduction/re-oxidation cycle was repeated twice to evaluate the long-term stability.

TP reductions allow the testing of the catalysts' activity and selectivity without the disturbing gas phase oxidation and the quantification of lattice oxygen incorporated in each oxidation product (AA, CO, CO_2, H_2O). Below 200 °C the mixed oxides are inactive. Activity rises slowly up to 300 °C and remains constant until a steep increase starts at about 420 °C. Activity drops as soon as the lattice oxygen is consumed.[11,23,31]

TP reductions confirm that catalysts with a molar ratio of Mo/V of 3 exhibit the best performance.[11,23]

The integral evaluation of the AA production (Fig. 6) shows the influence of the drying method and that W does not only serve as structural promoter but influences selectivity and activity significantly. These results are proven with TP reactions and isotope exchange experiments and will be discussed in detail in the following sections.

In situ XAS analysis of the catalyst under reductive conditions has been carried out for the V K-edge, the Mo K-edge and the W L_2-edge. The oxidation states of the constituent metal ions were determined from the energy shift of characteristic XANES features by means of energy shift scales.[22,38] Sample *in situ* spectra are shown in the electronic supplementary information (Fig. S1 and S2).† While both V and Mo ions can be reduced in atmospheres containing 5 vol% ACR in He, W remains inert against reduction. W instead seems to promote the reduction of V ions. In the presence of W, the

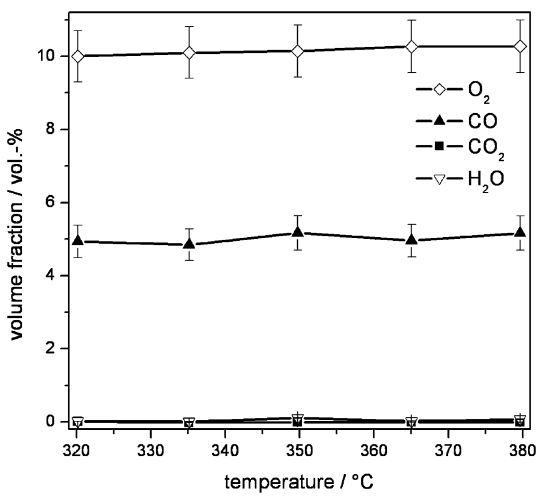

Fig. 5 Concentration profile of the steady state reaction at different temperatures with $V_2M_8W_{0.5}O_z$; m_{cat} = 50 mg, feed composition 5% (L L^{-1}) CO and 10% (L L^{-1}) O_2 in Ar, 320 ≤ T ≤ 380 °C.

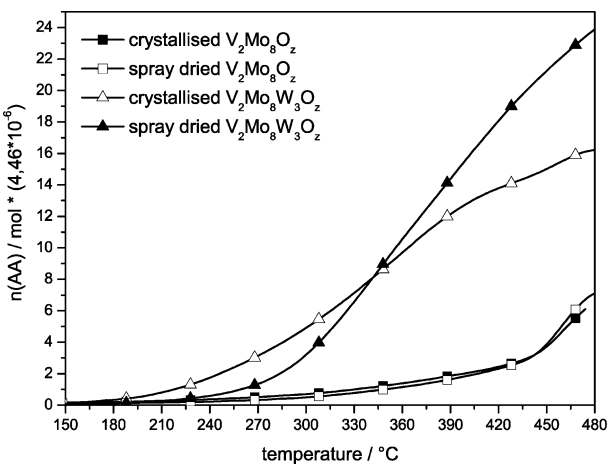

Fig. 6 Integral evaluation of AA production during TP reductions. The positive influence of the spray-drying method and W-doping is shown.

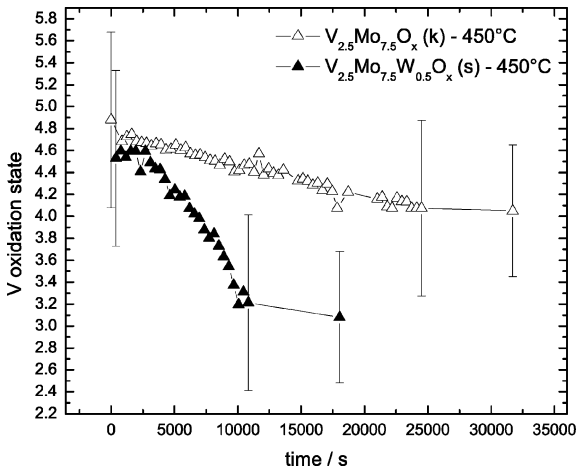

Fig. 7 Reduction of V ions in a W-free (open symbols) and a W-containing (closed symbols) catalyst. In catalysts without W, the minimum vanadium oxidation state is V^{4+}, while for catalysts with W, V^{3+} is reached.

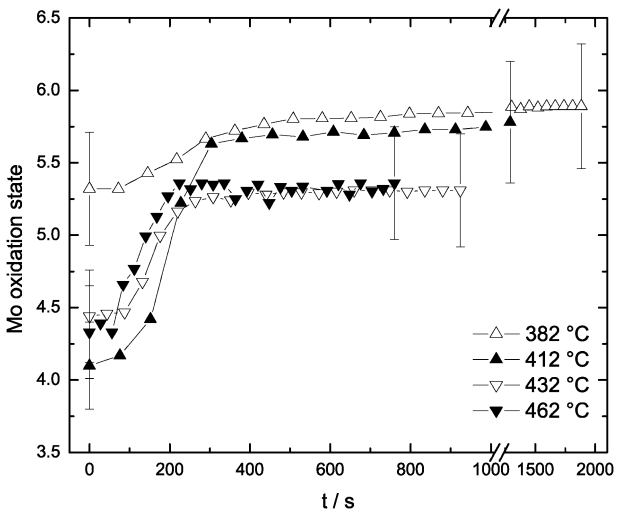

Fig. 9 Re-oxidation of Mo ions in the catalyst $V_{2.5}Mo_{7.5}O_z$.

minimum oxidation state for V ions changes from V^{4+} to V^{3+} (Fig. 7).

The reactivity of Mo ions during reduction has been studied at temperatures between 382 and 462 °C (Fig. 8). It seems that at around 400 °C a severe change in mechanism takes place. The data at 382 °C show only a very slight decrease in oxidation state from 5.6 to 5.3, coupled with small structural changes around the Mo centres. This is compatible with the proposals of Andrushkevich[14] and Schlögl *et al.*[15,16] for possible active phases in the catalyst. At temperatures above 400 °C, the change of oxidation state is much more drastic, and average minimum oxidation states close to Mo^{4+} are reached. This is consistent with the structural changes around the Mo centres. The reduced structure very closely resembles the structure of MoO_2.

Re-oxidation of the catalysts with 20 vol% O_2 in He shows a good cyclability of the samples (Fig. 9). Especially for the W-containing samples, the initial state is restored almost completely after re-oxidation. The characteristic time for re-oxidation is around a factor of 5–10 faster than the characteristic time for reduction.

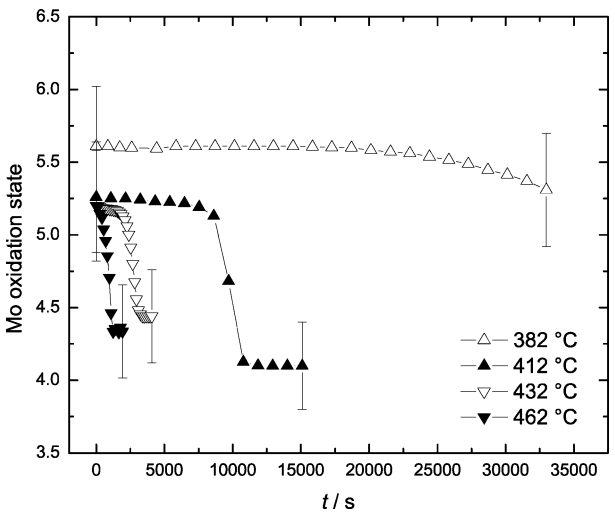

Fig. 8 Reduction of Mo ions in the catalyst $V_{2.5}Mo_{7.5}O_z$ (s).

In the usual transmission mode of XAS only bulk phenomena can be analysed. However, at conditions of maximum selectivity towards acrylic acid (up to 350 °C), the amount of bulk participation in the catalytic reaction is unclear; and the catalysts' surface and sub-surface are assumed to play an important role. In principle, direct analysis of these regions is possible by means of surface sensitive XAS techniques. This is not feasible with the present catalyst samples as smooth and well-defined surfaces would be required. Therefore, we will take another approach: careful evaluation of the thermal dependence of the bulk reduction and re-oxidation reactions at higher temperatures (380–460 °C), together with a model for the reaction kinetics of each of the reaction steps will be used to extrapolate the catalyst's performance to those lower temperatures of best selectivity (300–350 °C).[39]

Post-mortem characterisation. The XRD patterns of the crystalline samples of both hydrochemical preparation series show crystalline structures after a reduction–oxidation–reduction cycle with an ACR-containing atmosphere as described above. However, a complete change in the phase composition is observed. Instead of $(V,Mo)O_3$ and $(V,Mo)_2O_5$ reduced compounds with monoclinic MoO_2, SG $P2_1$,[40] and monoclinic VO_2 structure types, SG $C2/m$,[41] are found as main phases. The structure types of the minor phases are orthorhombic MoO_3, hexagonal WO_3 and monoclinic MoO_3, SG $P2_1/c$.[42]

For the spray-dried samples the preference lies on MoO_2. Only small amounts of other phases are found, in particular VO_2.

For the samples with amorphous/nanocrystalline structures with W contents of $3 \leq y \leq 5$ no change in crystallinity can be observed. VO_2 as a part of the phase composition is proven. Mo_5O_{14} and MoO_3 seem to be stable against the reduction process. This can be explained by the stabilisation of thermodynamically metastable phases by tungsten[9] and the inertness of small particles against reduction as Leisegang *et al.* have shown for the reduction of MoO_3 to MoO_2 by hydrogen.[43]

The reduction mechanism of the main phases, hexagonal $(V,Mo)O_3$ and tetragonal Mo_5O_{14}, has to be considered separately. For hexagonal $(V,Mo)O_3$ a direct reduction to MoO_2 is expected which is in agreement with the literature.[38,44,45] Mo_5O_{14} is stable because the reduction temperature is limited to 480 °C. The disproportion of V- and W-doped Mo_5O_{14} to MoO_3 and MoO_2 is observed at temperatures $\geq$ 547 °C.[46]

The re-oxidation of the reduced crystalline samples of both hydrochemical preparation methods in air again results in XRD patterns with crystalline structures. But a reconstruction of the hexagonal $(V,Mo)O_3$ structure type found before reduction fails. Reduced phases like MoO_2 or VO_2 are totally oxidised. The structure types found after re-oxidation are triclinic $(V,Mo)_2O_5$ for the W content $y = 0$ and hexagonal WO_3 for $y \geq 1.5$. The new phases detected for the crystalline samples are the structure types of orthorhombic MoO_3, SG *Pnma*,[47] tetragonal Mo_5O_{14}, SG $P4/mbm$,[33] monoclinic MoO_3, SG $P2_1/c$,[42] and orthorhombic $Mo_{0.6}W_{0.4}O_3$, SG $Cmc2_1$.[27]

The amorphous/nanocrystalline catalysts with W contents of $y > 3$ show the same structural behaviour like the freshly prepared and calcined catalysts with phases of the orthorhombic MoO_3 and tetragonal Mo_5O_{14} structure types.

"Reactive" conditions

***In situ* characterisation.** The performance of the catalysts under industrially relevant conditions (pressure, feed composition, (temperature)) was characterised by TP reactions, conducted in the microreactor described above. 50 mg of a probe were pre-treated at 400 °C for 60 min with 10 vol% oxygen (Messer Griesheim) in inert gas with a flow rate of 1.2 l h^{-1} and subsequently cooled down to room temperature in inert gas. Argon (Messer Griesheim) was used as the inert gas. The TP reaction was carried out with 10 vol% oxygen and 5 vol% ACR (BASF), balance argon. The temperature was raised with a constant heating rate of 10 °C min^{-1} to a maximum of 480 °C and cooled down to 400 °C followed by a re-oxidation of the catalyst under the conditions of the pre-treatment. The reaction/re-oxidation cycle was repeated twice to evaluate the long-term stability.

The samples of the solid state reaction with the thermodynamically stable phases do not influence the reaction of ACR to AA positively. When conversion of ACR starts at 400 °C only total oxidation products are detected.[23,31]

A typical concentration profile with a spray-dried model catalyst ($V_2Mo_8W_3O_z$) is presented in Fig. 10. Below 250 °C there is almost no conversion of ACR, then the production of AA and combustion products occur simultaneously. The concentration of AA reaches its maximum between 350 and 420 °C depending on the catalysts' composition.

As a measure of the catalysts' performance, selectivity, conversion and yield were calculated from the gas phase analysis. Neither pure molybdenum oxide nor pure vanadium oxide is suitable as model catalyst for AA production. The best Mo/V ratio was found to be between 3 and 4. A comparison of spray-dried and crystallised samples clearly shows that amorphous structure parts are essential for catalysis, at least in ACR oxidation.[11]

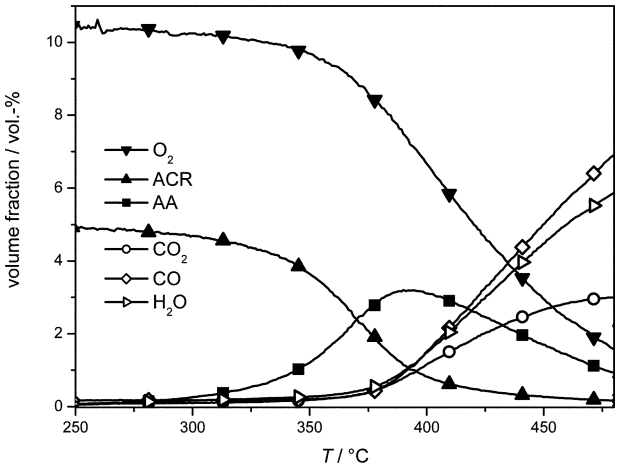

Fig. 10 Concentration profile of a TP reaction with $V_2Mo_8W_3O_z$; m_{cat} = 50 mg, 5 % (L L^{-1}) ACR and 10 % (L L^{-1}) O_2 in Ar, β = 10 K min^{-1}.

The influence of W doping arises in terms of the catalysts' long-term stability as indicated by the cyclic TP experiments. While the W-free catalyst is deactivating from cycle to cycle, the W-doped catalysts show, after a run-in process during the first cycle, a constant maximum of AA in the second and third cycles (Fig. 11).

The active and selective phases in the W containing samples are formed under reaction conditions. Especially at lower temperatures around 350 °C the minor W doped catalysts $V_2Mo_8W_yO_z$ with $0 \leq y \leq 5$ show the best performance in terms of activity and yield of AA. A selectivity to AA of around 80% at a ACR conversion of 80% was reached in TP reactions with 5 vol% ACR and 10 vol% O_2. According to the literature, yields of AA up to 90 vol% can be realised with water added to the feed gas.[48] However, the intention of our work was not to improve the catalytic performance but to reach a better scientific understanding of the catalytic system. The catalysts performance and dependence on the W content has been described in detail previously.[49]

Altogether, none of the pure oxides of Mo, V or W show the necessary characteristics of an active and selective catalyst. MoO_z is moderate in selectivity but almost inactive, VO_z instead shows high activity but is unselective. WO_z is inert. Catalysts with a varying ratio of Mo/V were found to be active and selective but an amorphous long-term stable model catalyst could only be obtained by doping with W.

XAS analysis at the Mo K-edge was also carried out under "reactive", steady state conditions, *i.e.* using 10 vol% O_2 and 5 vol% ACR in He carrier gas. The oxidation state and structure around the Mo ions is almost indistinguishable from the oxidised state, the total degree of reduction does not exceed 10%.[39]

Post-mortem characterisation

For the reaction of ACR to AA the catalysts are oxidised primarily. In the second step the ACR oxidation is performed.

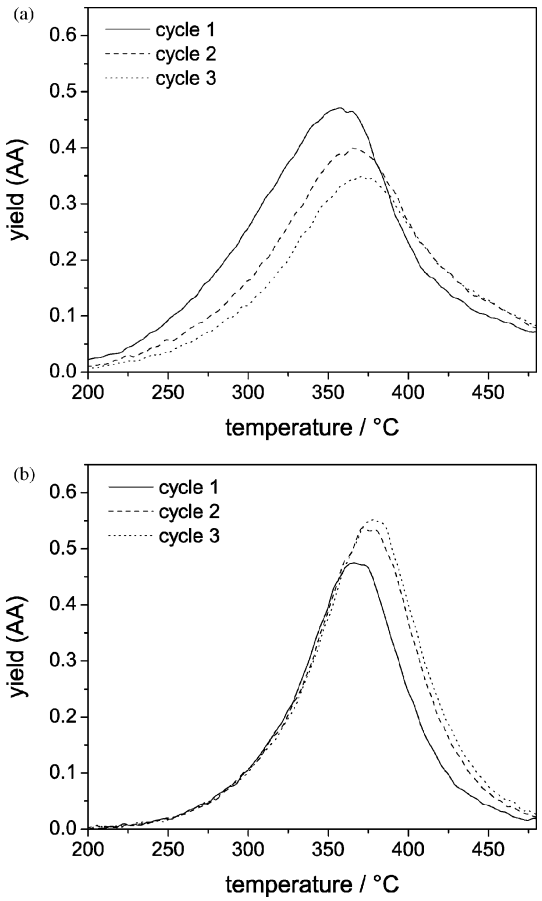

Fig. 11 Yield of AA in cyclic TP experiments. The W-free catalyst $V_{2.5}Mo_{7.5}O_z$ (top) is deactivating from cycle to cycle, the W-doped $V_{2.5}Mo_{7.5}W_{0.5}O_z$ (bottom) shows a constant maximum in the yield of AA in the second and third cycle.

The oxidation in air and subsequently the reaction of ACR in air are discussed combined with the structural changes in this section. The oxidation is carried out at different temperatures from RT to 450 °C (Fig. 12) on catalysts prepared using both hydrochemical preparation methods after the calcination procedure.

At room temperature the phase composition of the crystallised sample with a W content of $y = 1$ is exactly the same as determined before. The first transformation is the decrease of the phases with triclinic $(V,Mo)_2O_5$ and hexagonal WO_3 structure types. An increase of hexagonal $(V,Mo)O_3$ and tetragonal Mo_5O_{14} is observed at 380 °C after 1 h. The oxidation at 400 °C for the same time period causes a much higher transformation rate towards Mo_5O_{14} which culminates in the highest amount of Mo_5O_{14} at 450 °C. At this temperature the deactivation of the catalyst by thermodynamically stable phases begins and is continued at 500 °C for 6 h until all phases are characterised by their thermodynamic stability, except the minor phase of thermodynamically metastable monoclinic MoO_3. $V_2Mo_8W_1O_z$ was oxidised at 500 °C to show the possibility of the formation of thermodynamically stable phases in the phase composition of hydrochemically (instead of solid state) prepared catalysts. The XRD patterns still show crystalline structures but a phase transformation is

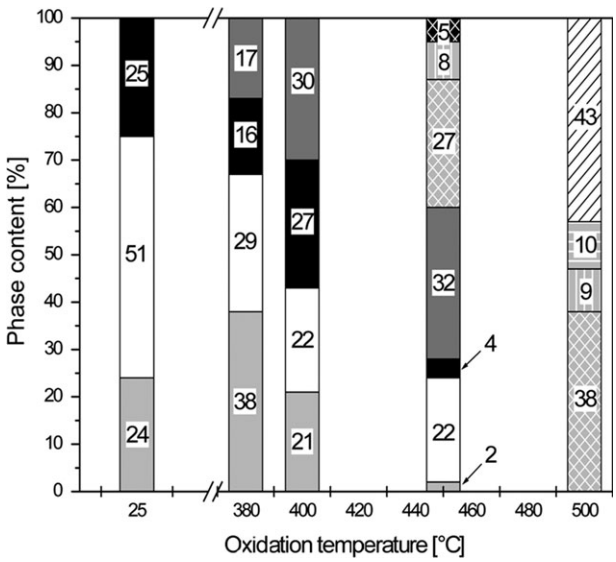

Fig. 12 Phase transformation during oxidation with air at different temperatures of $V_2Mo_8W_1O_z$ prepared from a crystallised precursor. hexagonal $(V,Mo)O_3$, triclinic $(V,Mo)_2O_5$, hexagonal WO_3, tetragonal Mo_5O_{14}, orthorhombic MoO_3, orthorhombic $Mo_{0.6}W_{0.4}O_3$, monoclinic $Mo_{0.21}W_{0.71}O_3$, orthorhombic V_2MoO_8, monoclinic MoO_3.

observed. All thermodynamically stable phases obtained by oxidation are described in the corresponding phase diagrams.[10,27]

Similar results are observed for the crystallised samples with tungsten contents $y > 1$. There, the formation of some phases like monoclinic MoO_3 or triclinic and orthorhombic WO_3 depends on the amount of added tungsten.

The spray-dried sample with $y = 1$ shows a similar behaviour in the phase transformation but the speed seems to be much faster than for the crystallised samples. Three-quarters of the phase content is represented by Mo_5O_{14} whereas the amount of the hexagonal $(V,Mo)O_3$ structure type decreases from above 50% to 25%. No other phases are identified. At 450 °C a deactivation by thermodynamically stable phases of orthorhombic MoO_3 and $Mo_{0.6}W_{0.4}O_3$ structure types is observed. The stabilisation effect of W and of the smaller particles compared to the crystallised samples inhibit a faster deactivation which is supported by the literature.[9,43]

For spray-dried samples with W contents $y > 2$ the phase composition seems to be stable against phase transformation under the investigated conditions.

ACR with a concentration of 5 vol% in the reaction gas seems to have only negligible effects on the phase transformations. The difference in the phase contents, especially the formation of thermodynamically stable phases, can be related to the longer heating period of 2 h instead of 1 h. The possibility of this further transformation to thermodynamically stable phases is shown for the crystallised sample with $y = 1$ conditioned at 500 °C for 6 h without ACR (Fig. 12).

However, reaction and subsequent re-oxidation affect the oxidation states especially of vanadium near the surface as indicated by XPS. An increase in the amount of V^{4+} is observed after the reaction (Tables 1 and 2). The amount of

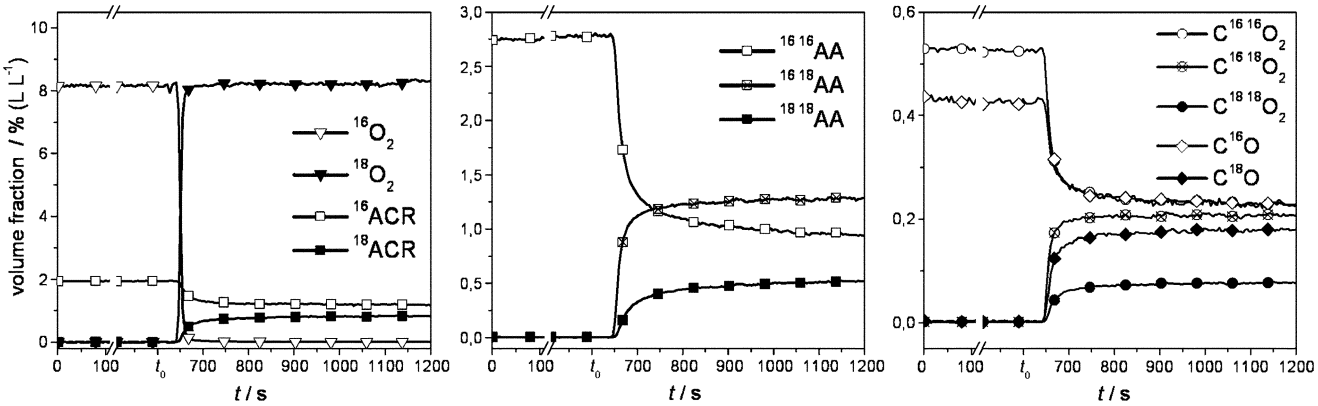

Fig. 13 SSITKA with $V_2Mo_8W_3O_z$; transient responses of ACR, AA, CO and CO_2 after the abrupt change from $^{16}O_2$ to $^{18}O_2$ in the feed gas.

V^{5+} increases after re-oxidation but stays below the value of the as-prepared catalysts. Mo and W cations are stable against changes in the oxidation state which remains at +6 for both elements. No other oxidation states are observed. These results are consistent with those of the XAS and XRD measurements.

Oxygen pathways

The oxygen pathways were investigated with steady state isotopic transient kinetic analysis (SSITKA). Under steady state conditions $^{16}O_2$ is abruptly replaced with $^{18}O_2$, the response of the system is monitored by mass spectrometry. The rate of oxygen incorporation into the reactants and the isotopic distribution of the oxidation products in dependence on the temperature and the W content was analysed. The resulting reaction profiles (Fig. 13) are similar for each catalyst and are described elsewhere.[50] The main aspects are as follows: Acrolein (^{16}ACR) itself is able to exchange carbonyl oxygen with oxygen from the solid, so isotopically labelled acrolein (^{18}ACR) is produced.

$$^{16}\mathrm{ACR} + [^{18}\mathrm{O}]_s \rightarrow {}^{18}\mathrm{ACR} + [^{16}\mathrm{O}]_s$$

Hence, for AA all three possible isotopomers (^{16} ^{16}AA, ^{16} ^{18}AA and ^{18} ^{18}AA) were detected. The total oxidation products appear with all kinds of isotopomers (^{16}CO, ^{18}CO, $C^{16}O_2$, $C^{16}O^{18}O$, $C^{18}O_2$, $H_2{}^{16}O$, $H_2{}^{18}O$). The transient response of oxygen is as fast as the transient response of the inert tracer He and no $^{16}O^{18}O$ was detected. Therefore, oxygen does not adsorb reversibly on the catalyst surface.

The slope of the other transient responses is characterised by a rapid decrease of the unlabelled components followed by a very slow decrease which is not terminated after 10 min. This phenomenon can be described by the fast replacement of the unlabelled intermediates on the catalyst's surface and a slow depletion of ^{16}O from the catalyst's bulk. By calculating the mass balance of the isotopic distribution the quantification of the oxygen released by the catalyst is possible. SSITKA with a series of catalysts containing an increasing amount of W ($V_2Mo_8W_yO_z$ with $0 \leq y \leq 5$) shows clearly the influence of W. The catalysts with minor W content release the highest amount of ^{16}O. In accordance with the results of the TP experiments high conversion of ACR (Fig. 14) correlates with the amount of lattice oxygen made available by the catalysts (Fig. 15). The maximum of activity in ACR oxidation is found for the catalyst with a W content of $y = 1$. W doping raises the mobility of oxygen by preventing the agglomeration of edge-sharing metal oxygen octahedrons and therefore formation of shear structures. Obviously a small W content suits this purpose whereas with increasing W contents the amount of inert, redox stable material is increased. However, a second maximum of activity is found for a W content of $y = 3$. This is consistent with results from XRD which indicate a stabilisation of amorphous/nanocrystalline structures for samples with W contents $y > 2$.

Because the transient response of ACR indicates complex adsorption and desorption processes on the surface, SSITKA with the products was performed to implement their reactions in the model if necessary. AA exchanges carboxylic oxygen with the solid oxygen and is converted to the combustion products, while CO is not activated for oxidation to CO_2. In the investigated temperature range (315–375 °C) none of the total oxidation products CO, CO_2 or water exchange oxygen with the catalyst.

Models for bulk and reaction

From the results for the solid state characterisation described above, a model for the reaction of the bulk is developed.

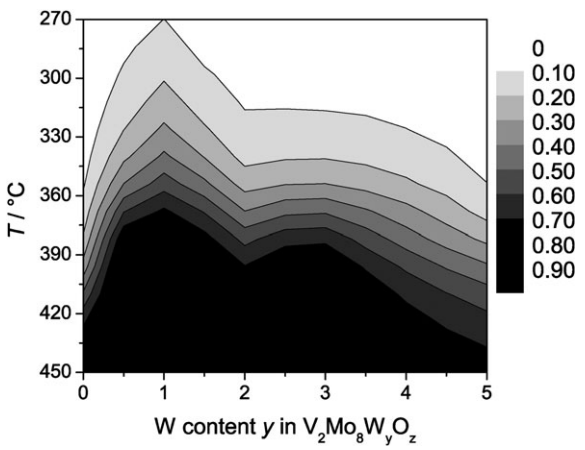

Fig. 14 Conversion of ACR in dependence on temperature and a varying W content y in $V_2Mo_8W_yO_z$.

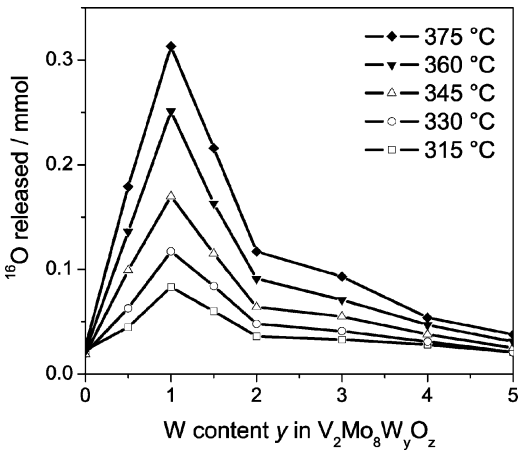

Fig. 15 Amount of oxygen released by the catalysts of the W-variation ($V_2Mo_8W_yO_z$), derived from SSITKA. For determination of the oxygen mobility a mass balance was drawn (^{16}O measured in all components at the reactor outlet minus ^{16}O from ACR in the feed).

Fig. 16 symbolises the influence of the oxidation reaction of ACR to AA in a simple, but absolutely sufficient way. First of all, it describes the ground state of the calcined catalysts before reaction. This is represented by the phases of the crystalline samples determined by XRD and TEM. The integration of all cations in the construction of the phases are shown by an energy-dispersive X-ray spectroscopy (EDXS) mapping in a scanning electron microscope (SEM) and TEM. These results are not shown, because these are well known features of the catalysts, especially for the spray-dried samples.[9,51]

The reactions are combined in the arrows and the phase transition area with the common stoichiometry $(VMoW)O_z$. For the arrows a decomposition and a partially reconstructive transition of phases is observed. In principle the hexagonal $(V,Mo)O_3$ structure is destroyed during the reaction as represented by the one-way arrows. The triclinic $(V,Mo)_2O_5$ and hexagonal WO_3 structure types are partially or totally decomposed and can be reconstructed under oxidising conditions as represented by the two-way arrows. The phase transition area also represents the formation of the tetragonal Mo_5O_{14} structure type. In many publications it is described as the phase responsible for the catalytic activity towards ACR oxidation to AA.[21,34,43,46,52,53] As shown in the recent sections the re-oxidation of the reduced catalysts and the treatment under oxidising/reactive conditions always force the formation of Mo_5O_{14} which is stable in dependency on the particle size.[43] The decomposition of Mo_5O_{14} only sets in at temperatures >430 °C.[31,51]

For the spray-dried amorphous/nanocrystalline catalysts the model possesses a similar validity, but the phases have to be replaced by the corresponding phases of this system. The phase transition area (Fig. 16) in this case highly depends on the time and temperature for the organisation of the phases and therefore a maximal catalytic activity towards AA formation of these samples. The phase transition area can also be seen as the area of the reduced and re-oxidised phases and the area of migration of the cations. The reconstruction of phases is also possible for the totally reduced catalysts during re-oxidation. The observed phase transformations in this system depend on reaction time, reaction temperature, and elemental composition as well as on the preparation method.

The kinetics of the partial oxidation of ACR to AA on V–Mo–W mixed oxide catalysts as well as the oxygen pathways were studied using transient isotopic tracing. After switching from $^{16}O_2$ to $^{18}O_2$ the formation of ^{18}O-labelled ACR was observed. This is due to a fast exchange reaction of the carbonylic oxygen of ACR involving lattice oxygen from the catalyst. Subsequent desorption of ACR, as well as further reaction to the oxidation products, can take place. As a result, the formation of doubly labelled AA occurs.

Measurements at various temperatures were performed to collect kinetic data. Based on the experimental data of all gaseous reactants involved (ACR, AA, O_2, CO, CO_2, H_2O) and the isotopic pattern, a reaction model could be developed which describes the oxygen exchange and the processes at the catalyst more precisely (Fig. 17). In addition, the results of model simulations (coupled with a parameter estimation routine) give statements concerning the rate limiting steps and their activation. The simulation results which have been published recently are summarised in Table 3.[50]

Modelling of the SSITKA provides an opportunity to obtain some activation parameters, which are inaccessible with ordinary steady state kinetics. Thus, the activation energy of the exchange of the carbonylic oxygen of ACR was determined to be approximately 30 kJ mol^{-1}.

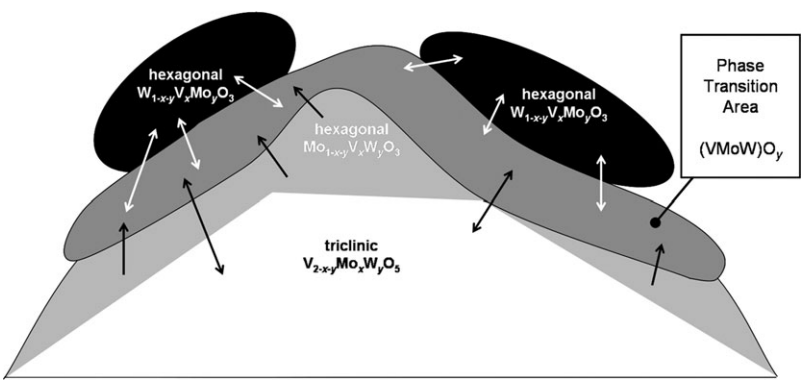

Fig. 16 Bulk model of the solid for different reaction conditions in the presence and absence of ACR.

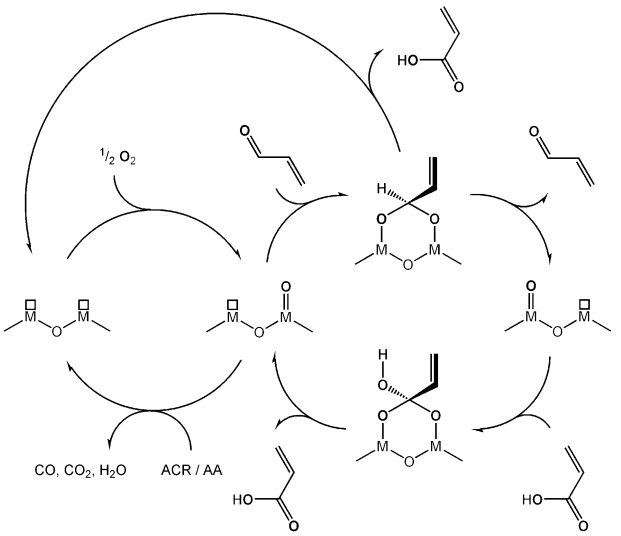

Fig. 17 Catalytic cycle for the oxidation and oxygen exchange reactions of ACR and AA.

Conclusion

The main intention of this work was to elucidate the structure, function and dynamics of V–Mo–(W) mixed oxides in the selective oxidation of ACR to AA. Therefore, in the context of the DFG priority programme "Bridging the gap between ideal and real systems in heterogeneous catalysis" a less complex model system for the commercial catalyst was derived from evaluation of the catalytic performance in combination with structure research. However, in the case of this kinetically demanding reaction system the gap from an idealised single crystal under UHV to the complex catalyst under working conditions cannot be bridged completely.

The most important influences on the catalysts' performance are the preparation method, the reaction atmosphere, and the temperature.

Solid state and hydrochemical preparation methods led to different crystallinity in the $V_2Mo_8W_yO_z$ system. Dependent on the W content, thermodynamically stable and metastable crystalline or amorphous to nanocrystalline phases are formed. While the thermodynamically stable phases do not show a significant conversion of ACR to AA, the hydrochemically prepared catalysts show a high activity towards AA production. The reaction conditions strongly influence the formation of new phases. Thus, the phases of the prepared mixed oxides are not necessarily the catalytically active ones. The catalyst is formed under the reaction conditions. Extracted from the results above, a special reaction scheme shows

Table 3 Kinetic data from Arrhenius plots of SSITKA with $V_{2.5}Mo_{7.5}W_{0.5}O_z$ at different temperatures (315 °C $\leq T \leq$ 375 °C)

	k_0/L mol^{-1} s^{-1}	E_A/kJ mol^{-1}
^{16}ACR $\rightleftharpoons$ ^{18}ACR	35.0	30
ACR → AA	31.6×10^8	119
ACR → CO_2	35.4×10^6	108
ACR → CO	33.5×10^{10}	153
[ ]$_s$ → [O]$_s$	39.3×10^8	110

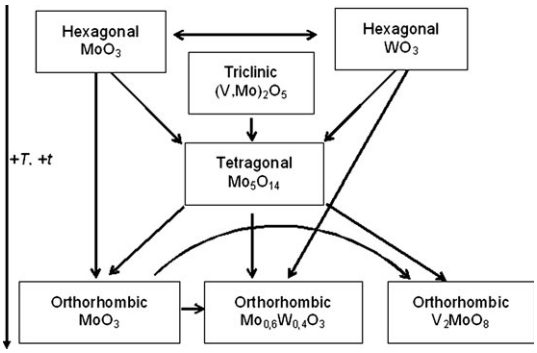

Fig. 18 Possible phase transformations of the solid during oxidation and reaction in dependence on temperature and time.

the logical, possible and effective phase transformations in the V–Mo–W mixed oxide catalysts during the oxidation–reaction cycles (Fig. 18). Only the spray-dried catalysts with a W content of $y > 2$ remain stable. The V–Mo–W mixed oxides presented in this work are able to form Mo_5O_{14}—one of the proposed structures with high catalytic activity and selectivity towards AA[9,46,52]—independently from the initial phases (as long as they are not thermodynamically stable or highly crystalline). Opposite to the pure oxides of Mo, V and W the mixed oxides of V–Mo are selective and active in oxidation of ACR, but only doping with W results in active, selective and stable catalysts. The best catalysts are located at a range of W contents in which the highest Mo_5O_{14} concentrations are found as well.

Analysis of the catalyst under reaction conditions, directly by XAS, and indirectly by modelling nonstationary reduction and re-oxidation data, shows a very low degree of reduction between 0 and 10% for the working catalyst. Different time scales for catalysis and bulk redox cycles have been found.

The oxidation state of Mo during reduction at 380 °C is quite stable around 5.5. This is very close to the oxidation state of Mo_5O_{14}. At higher temperatures, this stability breaks down, and molybdenum oxide is reduced to a MoO_2-analogue structure. The oxidation state of V during reduction is strongly influenced by the composition of the catalyst. In the presence of W, V can be reduced to a V_2O_3-type phase, while in a W-free catalyst, only a VO_2-type phase can be reached.

The comparison of induction delays for the nonstationary reduction indicates, that at the beginning of the reaction, almost all oxygen is taken from the coordination shells around the V ions. The reduction of Mo finally starts, after the V ions are reduced to a certain level. This also indicates, that the active phase incorporates Mo at an average oxidation state around 5.3–5.5, while the oxygen is taken from reducing a V_2O_5-analogue phase.

The kinetics of the partial oxidation of ACR to AA with V–Mo–W mixed oxide catalysts was studied using transient isotopic tracing. In the SSITKA experiments, $^{16}O_2$ in the feed gas was abruptly exchanged against $^{18}O_2$ under steady state reaction conditions. A fast exchange reaction of the carbonylic oxygen of ACR involving lattice oxygen from the catalyst was observed. Subsequent desorption of ACR as well as further reaction to the oxidation products can take place. As a result, the formation of doubly labelled AA occurs. SSITKA at

various temperatures were performed to collect kinetic data. The kinetic parameters were obtained by fitting a macrokinetic model (Fig. 17) to the experimental values. Modelling of the SSITKA results provides an opportunity to obtain some activation parameters, which are inaccessible with ordinary steady state kinetics. Thus, the activation energy of the exchange of the carbonylic oxygen of acrolein was determined to be approximately 30 kJ mol^{-1}.

Tungsten doping has a significant influence on the oxygen mobility as proven by the different amounts of unlabelled oxygen removed from each catalyst under $^{18}O_2$. This is also consistent with the *in situ* XAS analysis. Due to the stabilisation of lower-valence vanadium oxide phases in the presence of W, twice as much oxygen is available from these phases. The amount of oxygen made available by the catalyst correlates with the catalyst's activity. With an increasing W content ($y > 1$) on the one hand a stabilisation of amorphous/nanocrystalline structures is reached but on the other hand the amount of inert, redox stable material is increased.

By investigating this model system with different *in situ* methods a better understanding of the catalytic mechanism could be achieved. The derived models for the phase transformations in the catalysts and the reactions between the gas phase and the surface (Fig. 16–18) are capable of representing the experimental results.

However, more work has to be done to answer technically relevant questions as *e.g.* the influence of water (reaction water) on the catalytic mechanism. Furthermore, the modelling of the SSITKA experiments should be done with various metal compositions of the catalyst in order to connect the activation of ACR directly to structural information of the catalyst.

Acknowledgements

For financial support the German Research Foundation (DFG) SPP 1091 ''Bridges between real and ideal systems in heterogeneous catalysis'' is gratefully acknowledged.

References

1 S. Schulze and H. Vogel, *Chem. Eng. Technol.*, 1998, **21**, 829.
2 H. J. Arpe, in *Industrielle Organische Chemie*, Wiley-VCH, Weinheim, 6th edn, 2007, p. 321.
3 K. Winnacker and L. Küchler, in *Chemische Technik—Prozesse und Produkte*, Wiley-VCH, Weinheim, 5th edn, 2005, vol. 5, p. 210 f.
4 Ullmann's Encyclopedia of Industrial Chemistry, VCH, Weinheim, 5th edn, 1992, vol. A1, p. 165.
5 P. Mars and D. van Krevelen, *Spec. Supp. Chem. Eng. Sci.*, 1954, **3**, 41.
6 R. Schlögl, A. Knop-Gericke, M. Hävecker, U. Wild, D. Frickel, T. Ressler, R. E. Jentoft, J. Wienold, G. Mestl, A. Blume, O. Timpe and Y. Uchida, *Top. Catal.*, 2001, **15**, 219.
7 R. K. Grasselli, J. D. Burrington, D. J. Buttrey, P. DeSanto, Jr, C. G. Lugmair, A. F. Volpe, Jr and T. Weingand, *Top. Catal.*, 2003, **23**, 5.
8 P. Concepcion, P. Botella and J. M. Lopez Nieto, *Appl. Catal., A*, 2004, **278**, 45.
9 G. Mestl, C. Linsmeier, R. Gottschall, M. Dieterle, J. Find, D. Herein, J. Jaeger, Y. Uchida and R. Schlögl, *J. Mol. Catal. A: Chem.*, 2000, **162**, 463.
10 V. L. Volkov, G. S. Tynkacheva, A. A. Fotiev and E. V. Tkachenko, *Russ. J. Inorg. Chem.*, 1972, **17**, 1469.
11 J. Kunert, PhD Thesis, Darmstadt University of Technology, 2003.
12 J. Kunert, A. Drochner, J. Ott, H. Vogel and H. Fuess, *Appl. Catal., A*, 2004, **269**, 53.
13 R. Krabetz, W. Ferrmann, H. Engelbach, P. Palm, K. Sommer and H. Spahn, Eur. Pat., 0017000, 1980.
14 T. V. Andrushkevich, *Catal. Rev. Sci. Eng.*, 1993, **35**, 213.
15 H. Werner, O. Timpe, D. Herein, Y. Uchida, N. Pfänder, U. Wild, R. Schlögl and H. Hibst, *Catal. Lett.*, 1997, **44**, 153.
16 Y. Uchida, G. Mestl, O. Ovsitser, J. Jäger, A. Blume and R. Schlögl, *J. Mol. Catal. A: Chem.*, 2002, **187**, 247.
17 M. Dieterle, H. Hibst, W. J. Poepel, J. Petzoldt and K. J. Mueller-Engel, Eur. Pat., 1633478, 2006.
18 E. Bordes, *Top. Catal.*, 2001, **15**, 131.
19 R. K. Grasselli, *Top. Catal.*, 2001, **15**, 93.
20 R. K. Grasselli, *Top. Catal.*, 2002, **21**, 79.
21 G. Mestl, *Top. Catal.*, 2006, **38**, 69.
22 F. Haaß, A. H. Adams, T. Buhrmester, G. Schimanke, M. Martin and H. Fuess, *Phys. Chem. Chem. Phys.*, 2003, **5**, 4317.
23 A. H. Adams, F. Haass, T. Buhrmester, J. Kunert, J. Ott, H. Vogel and H. Fuess, *J. Mol. Catal. A: Chem.*, 2004, **216**, 67.
24 R. Enjalbert and J. Galy, *Acta Crystallogr., Sect. C: Cryst. Struct. Commun.*, 1986, **42**, 1467.
25 H. Eick and L. Kihlborg, *Acta Chem. Scand.*, 1966, **20**, 1658.
26 L. Kihlborg, *Ark.Kemi.*, 1963, **21**, 357.
27 E. Salje, R. Gehlig and K. Viswanathan, *J. Solid State Chem.*, 1978, **25**, 239.
28 Y. Hu and P. K. Davies, *J. Solid State Chem.*, 1993, **105**, 489.
29 L. M. Plyasova, L. P. Soloveva, S. V. Tsybulya, G. N. Kryukova, V. A. Zabolotnyi and I. P. Olenkova, *J. Struct. Chem.*, 1991, **32**, 89.
30 K. A. Wilhelmi, K. Waltersson and L. Kihlborg, *Acta Chem. Scand.*, 1971, **25**, 2675.
31 L. Giebeler, P. Kampe, A. Wirth, A. H. Adams, J. Kunert, H. Fuess and H. Vogel, *J. Mol. Catal. A: Chem.*, 2006, **259**, 309.
32 B. Gerand, G. Novogorocki, J. Guenot and M. Figlarz, *J. Solid State Chem.*, 1979, **29**, 429.
33 L. Kihlborg, *Ark. Kemi*, 1963, **21**, 427.
34 J. B. Wagner, D. S. Su, S. A. Schunk, H. Hibst, J. Petzold and R. Schlögl, *J. Catal.*, 2004, **224**, 28.
35 P. Kampe, Ph.D. Thesis, Darmstadt University of Technology, 2007.
36 G. Schimanke, M. Martin, J. Kunert and H. Vogel, *Z. Anorg. Allg. Chem.*, 2005, **631**, 1289.
37 R. Böhling, A. Drochner, M. Fehlings, D. König and H. Vogel, *Chem.-Ing.-Tech.*, 1999, **71**, 226.
38 T. Ressler, J. Wienhold, R. E. Jentoft and T. Neisius, *J. Catal.*, 2002, **210**, 67.
39 D. Samuelis and M. Martin, to be published.
40 A. Magneli, *Ark. Kemi, Mineral. Geol. A*, 1945, **19**, 1.
41 F. R. Theobald, R. Cabala and J. Bernhard, *J. Solid State Chem.*, 1976, **17**, 431.
42 J. B. Parise, E. M. McCarron III, R. B. von Dreele and J. A. Goldstone, *J. Solid State Chem.*, 1991, **93**, 193.
43 T. Leisegang, A. A. Levin, J. Walter and D. C. Meyer, *Cryst. Res. Technol.*, 2005, **40**, 95.
44 T. Ressler, O. Timpe, T. Neisius, J. Find, G. Mestl, M. Dieterle and R. Schögl, *J. Catal.*, 2000, **191**, 75.
45 T. Ressler, R. E. Jentoft, J. Wienhold, M. M. Günter and O. Timpe, *J. Phys. Chem. B*, 2000, **104**, 6360.
46 M. Dieterle, G. Mestl, J. Jäger, Y. Uchida, H. Hibst and R. Schlögl, *J. Mol. Catal. A: Chem.*, 2001, **174**, 169.
47 G. Andersson and A. Magneli, *Acta Chem. Scand.*, 1950, **4**, 793.
48 M. Sadakane, N. Watanabe, T. Katou, Y. Nodasaka and W. Ueda, *Angew. Chem., Int. Ed.*, 2007, **46**, 1493.
49 S. Endres, P. Kampe, J. Kunert, A. Drochner and H. Vogel, *Appl. Catal., A,* DOI: 10.1016/j.apcata.2007.02.040.
50 A. Drochner, P. Kampe, J. Kunert, J. Ott and H. Vogel, *Appl. Catal., A*, 2005, **289**, 74.
51 A. H. Adams, PhD Thesis, Shaker-Verlag, Aachen, 2004.
52 O. Ovsitser, Y. Uchida, G. Mestl, G. Weinberg, A. Blume, J. Jäger, M. Dieterle, H. Hibst and R. Schlögl, *J. Mol. Catal. A: Chem.*, 2002, **185**, 291.
53 S. Knobl, G. A. Zenkovets, G. N. Kryukova, O. Ovsitser, D. Niemeyer, R. Schlögl and G. Mestl, *J. Catal.*, 2003, **215**, 177.